On the effect of roughness parameters on adherence using the three-point bending test (ISO 14679:1997)

Thiago Birro, Eric Paroissien, Frederic Lachaud, Maëlenn Aufray

https://doi.org/10.1080/00218464.2021.2024808

On the effect of roughness parameters on adherence using the three-point bending test (ISO 14679:1997)

Thiago Vasconcellos-Birro[a,b], Eric Paroissien[a], Fréderic Lachaud[a], and Maëlenn Aufray[b]

[a]Institut Clément Ader (ICA), Université de Toulouse, Isae-supaero, INSA, IMT Mines ALBI, UTIII, CNRS, Toulouse, France; [b]CIRIMAT, Université de Toulouse, CNRS, INP- ENSIACET 4 allée Emile Monso - BP44362, Toulouse Cedex 4, 31030, France

ABSTRACT

In the present work, a specific three-point bending test is applied to evaluate how the roughness can impact the bond strength (adherence) and the mechanism of interfacial failure initiation. The study is conducted using an aluminum alloy 2024-T3 as substrate and the DGEBA (polyepoxide bisphenol A diglycidyl ether) /DETA (diethylenetriamine) as adhesive, considering different abrasive surface treatments. An optimal roughness is reached to maximize the critical force during failure initiation; besides, the roughness impacted the failure propagation mechanism and the failure initiation area for each abrasive treatment. A power-law regression is considered to correlate the critical force and the failure initiation area, considering different average roughness. Local assessment using a mechanical profilometer and Scanning Electron Microscope (SEM) with Focused Ion Beam (FIB) are applied to measure the residual adhesive thickness at failure initiation and failure propagation zones as well as the initiation-to-propagation transitions. It is constated that the residual adhesive thickness is dependent on the average roughness of the substrate. Finally, Weibull's analysis is undertaken to demonstrate that the mechanism of failure initiation for all substrate groups is essentially the same, although the failure propagation mechanism can be different.

KEYWORDS

Adhesively bonded joints; adhesive failure; three-point bending test; roughness; adherence

D_c	Critical displacement (mm)
f	Functionality
F_c	Critical force (N)
F_{P4000}	Average force for the group "P4000+diamond paste" (N)
j	Index of a sample
n	Total number of a group of sample
R_a	Average arithmetic of roughness (nm)
R_k	Core roughness depth (nm)
R_p	Maximum peak height (nm)
R_{pk}	Reduced peak height (nm)

CONTACT Maëlenn Aufray maelenn.aufray@ensiacet.fr Cirimat, Université de Toulouse, CNRS, INPT, UPS, 4, Allée Émile Monso -BP 44362, 31030 Toulouse Cedex 4, France +33534323442

R_q	Root-mean-square of roughness (nm)
R_t	Total height of the profile (nm)
R_v	Maximum valley depth (nm)
R_{vk}	Reduced valley depth (nm)
S_c	Failure initiation area (mm^2)
3PBT	Three-point bending test
CDF	Cumulative distribution function
C/PEEK	Carbon polyetherketoneketone
DETA	Diethylenetriamine
DGEBA	Diglycidyl ether
FIB	Focused Ion Beam
GLYMO	(3-Glycidyloxypropyl)trimethoxysilane
LSM	Least square method
MLM	Maximum likelihood method
PDF	Probability distribution function
phr	Parts per hundred of resin
SEM	Scanning Electron Microscope
SD	Standard deviation
ST	Surface treatment
WLSM	Weighted least square
Δy_{res}	Residual adhesive thickness (nm)

Nomenclature and units

1. Introduction

Over the years, diverse approaches have been developed to explain how adhesion works. However, none of those theories are considered the most correct, but they can be whether complementary or sometimes conflicting themselves.[1] McBain and Hopkinks (1926)[2] proposed the mechanical theory of adhesion as one of the first-ever theories. In this case, the adhesive attaches to the asperities of the substrate surface (mechanical interlocking). The theory is only valid when an intimate contact is well established between the polymer and substrate. Some studies in the 1950s showed the difficulty of getting a good wetting on rough surfaces for viscous adhesives, resulting in voids and the asperities acting as a point of stress concentration, as shown in Figure 1a and 1b. According to Packham (2011),[1] these voids are now avoided thanks to better adhesive wetting conditions. On the other hand, the mechanical theory of adhesion only is appropriate for rough surfaces when the contact is well-established (Figure 1b). Thus, different approaches are required to explain the adhesion for a very low roughness (see Figure 1c).

Considering the general aspects of the mechanical theory of adhesion, for Ye (1998)[2,3] and Packham (2002),[4] the morphology (roughness shape) of the substrate can be more determinant than the roughness parameters. Thus,

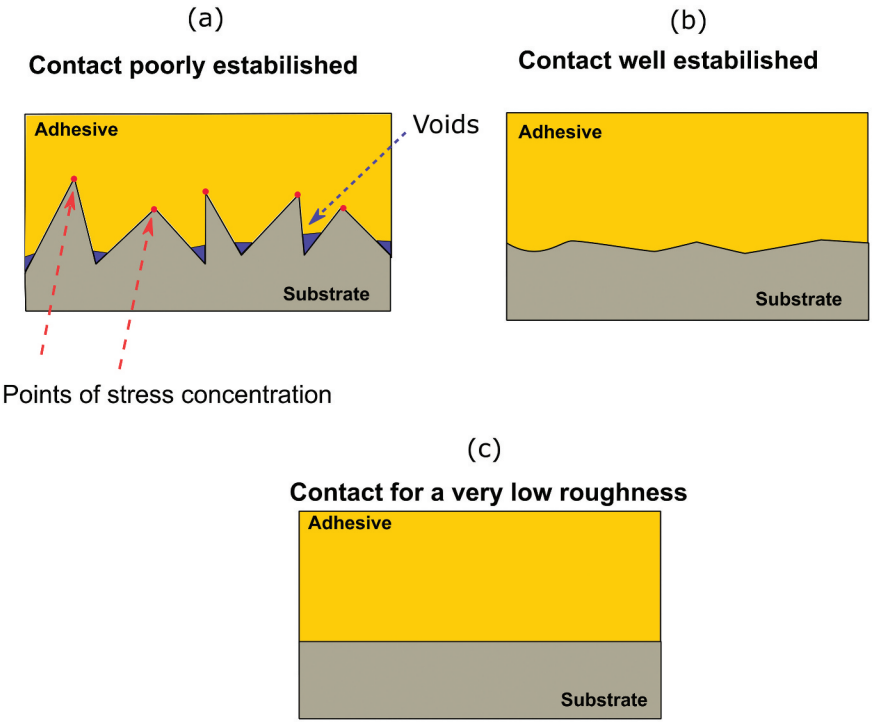

Figure 1. Region of intimate contact between adhesive/substrate.

optimum surface roughness can be reached, improving maximum strength for different mechanical tests. In order words, the bond strength does not increase as greater is the average roughness. Recent works have evaluated the impact of roughness and morphology on adhesively bonded joints during the last decades. For example, Cho et al. (2009)[5] analyzed the influence of the average arithmetic of roughness (R_a) on the adhesive strength using a single lap joint. The analysis was conducted based on a heat-resistant adhesive (RTV88) and aluminum adherends. In this case, the cohesive failure area increased as the surface roughness increased. On the other hand, they demonstrated that the shear stress decreased as the surface roughness increased until a specific critical value. Ghumatkar et al. (2016)[6] analyzed the contact angle and adherence, which is a synonym of bond strength according to,[7] on metallic adherends (mild steel and aluminum) bonded with an epoxy resin (Araldite® 2015) under different roughness conditions. The mechanical tests were carried out using a single strap joint. In such a case, optimal roughness, which was comprised between the minimum and maximum roughness, was reported for adherence. More recently, Marinosci et al. (2021)[8] analyzed the effect of grit-blasting on the mechanical properties of the interface using hybrid titanium-thermoplastic composite joints. A unidirectional carbon polyetherketoneketone (C/PEKK) tape was bonded

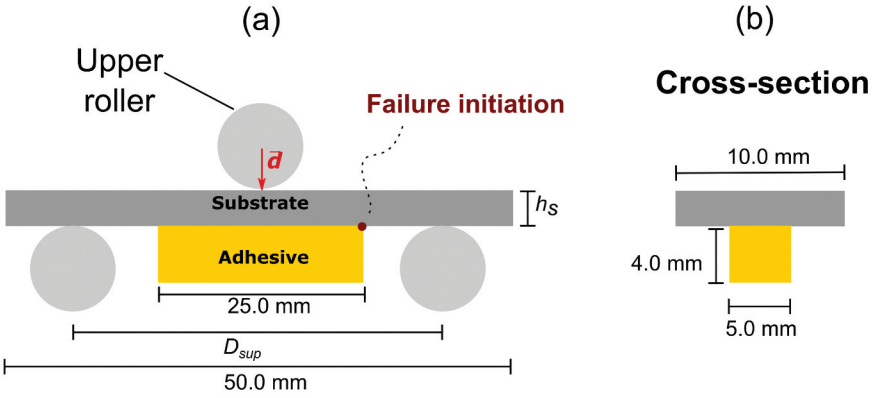

Figure 2. Dimension of 3PBT according to ISO 14679.[11].

into an aluminum adherend via mandrel peel test, in which mixed-mode fracture is possible. The peeled region possesses an interfacial failure for low surface roughness. Then, a roughness increase causes an increase of intraply failure leading to both interphasial and intraply failure. Marinosci et al. (2021)[8] have also analyzed the effect of roughness on fracture toughness. For low surface roughness, a low fracture toughness corresponded to interfacial fracture toughness. Then, fracture toughness increased as roughness increased until reaching the fracture toughness of an interlaminar failure.

Other factors associated with roughness can also promote an optimal bond condition, which maximizes adherence. For example, Paz et al. (2015)[9] argued that the wetting process also depends on the viscosity of the adhesive and the surface energy of adherend and adhesive. Paz et al. (2015)[9] demonstrated an optimal adherence value in terms of viscosity for an acrylic adhesive using lap-shear strength.

In all these examples, a complex task is associated with identifying the real adhesive failure initiation zone. Besides, these tests are associated with multiple interfaces since they correspond to sandwich configuration (adherend/adhesive/adherend).

For an accurate determination of the adherence, a specific three-point bending test (3PBT) proposed by Roche et al. (1982)[10] has been applied to assess adhesive failure. Genty et al. (2017)[11] demonstrated that the 3PBT had been shown as the most practical test to obtain an adhesive failure when compared with traditional sandwich joint configurations. According to ISO 14679,[12] the specimen comprises a stiff adhesive block (4 x 5 × 25 mm^3) bonded directly into the substrate (see Figure 2). Thus, a single metal-adhesive interface is obtained, contrary to the traditional tests (multiple interfaces).

The 3PBT is a particular test to assess adherence, which is classically expressed at the macroscopic scale in terms of maximal forces reached or energy dissipated. Recently, Birro et al.[13,14] suggested a methodology to assess the properties of the interface, regarded as a weak interface, in terms of stiffness, critical stress, and energy release rate. The methodology is based on an area at the interface created during failure initiation, which can be measured on the post mortem specimen. Nevertheless, a detailed analysis of the roughness influence has never been addressed. Hence, the present works aim to evaluate the roughness effect on the global mechanical response of the test as well as the adherence in terms of F_c.

2. Experimental test

2.1. Materials

For a better understanding of the general interaction between the adhesive and substrate, a model adhesive is selected for this specific study. The substrate is an aluminum alloy 2024-T3 laminated substrate (1.08 mm in thickness) supplied by Rocholl GmbH. The adhesive comprises a polyepoxide bisphenol A diglycidyl ether (DGEBA), functionality 2, supplied by DOW Chemical, and a diethylenetriamine (DETA), functionality 5, supplied by SIGMA–ALDRICH supplied the amine diethylenetriamine (DETA). The adhesion promoter GLYMO (3-Glycidyloxypropyl)trimethoxysilane, functionality one and supplied by SIGMA-ALDRICH, is also directly included in the adhesive formulation (*5 phr*). All compounds are mixed in the stoichiometric ratio $r = 1$, and their respective molar masses are $M_{DGEBA} = 340.41\ g$, $M_{DETA} = 170.30\ g$, and $M_{organ} = 236.34\ g$, respectively. Thus, the adhesive is produced by mixing the epoxy adhesion promoter at room temperature until the formation of a homogeneous phase. Then, the amine is included, mixing again at room temperature until forming a new homogeneous phase. Finally, the adhesive is fabricated using *0.5 mL* of liquid adhesive, as indicated in the manufacturing protocol (ISO 14679[12]). Once the adhesive is deposited into a silicone mold and wet substrate, the specimens stay 3 hours at room temperature and atmospheric pressure. The specific choice of three hours at room temperature provided is completely detailed in Section 3. Then, the temperature is increased gradually until the set-point temperature (140°C). The samples rest for one hour at the set-point temperature, followed by gradual cooling, avoiding residual stresses.

2.2 Substrate preparation

For evaluating the effect of surface roughness on adherence, the substrate is prepared under different roughness conditions. In this case, the abrasive treatment is performed manually using the polishing machine MINITECH-233 (PRESI SAS), considering other abrasive papers (P80, P320, P600, P1200, and P4000 + diamond paste) and a non-abraded group of samples. Eight substrates are prepared using each abrasive paper: a controlled protocol is chosen (80 rpm for 10 seconds) and imposed for a specimen. Furthermore, the controlled protocol is applied from 4 to 6 times, turning the sample into 180°. This setup allows a more uniform abrasion, ensuring the quality of the mechanical surface treatment. Subsequently, simple acetone degreasing is applied on the substrates, followed by a nitric acid etching, immersing the samples in a 6.3 *mol/L* solution at 50°C for 10 minutes. Finally, the samples are rinsed with de-ionized water and dried at room temperature.

All STs are evaluated immediately after being carried out using the mechanical profilometer. For each group, six 3D mappings are carried out directly after the chemical ST. Typical roughness profiles of each group are shown in Figure 3. In particular, the average roughness for a non-abraded substrate was previously presented by Birro et al. (2021).[13]

As can be noticed, rotatory marks are presented. Nevertheless, a small standard deviation is obtained for both the average arithmetic of roughness (R_a) and root-mean-square of roughness (R_q), as shown in Figure 4. Other details of general roughness parameters are also provided in Appendix A.

Thus, as shown in Table 1, a low standard deviation is obtained for all other parameters, ensuring good repeatability.

2.3. Three-point bending test (3PBT)

A typical scheme of the adhesive failure mechanism is demonstrated in Figure 5(a). A controlled displacement (0.5 mm/min) is imposed by the upper load. Thus, interfacial debonding is expected near the adhesive-substrate corner (see Figure 2) when the critical force (F_c) is reached at point B. Finally, the failure propagation occurs (BC) until the effect of the adhesive block disappears on the overall behavior (substrate stiffness CE). The dissipated energy (W_c) is defined as the subtended area (red area – see Figure 5(a)) between the overall stiffness (K_{over}) and the substrate stiffness (K_{subs}). Moreover, the reference system of axes is indicated in Figure 5(b) to facilitate the post-mortem analysis in the following sections.

An easily identified failure initiation zone is formed (see Figure 6) during failure initiation (point B – see Figure 5a), and it can be tracked via visual inspection. Birro et al. (2021)[13] demonstrated that the post-mortem analysis could present different configurations. In special, the small round area,

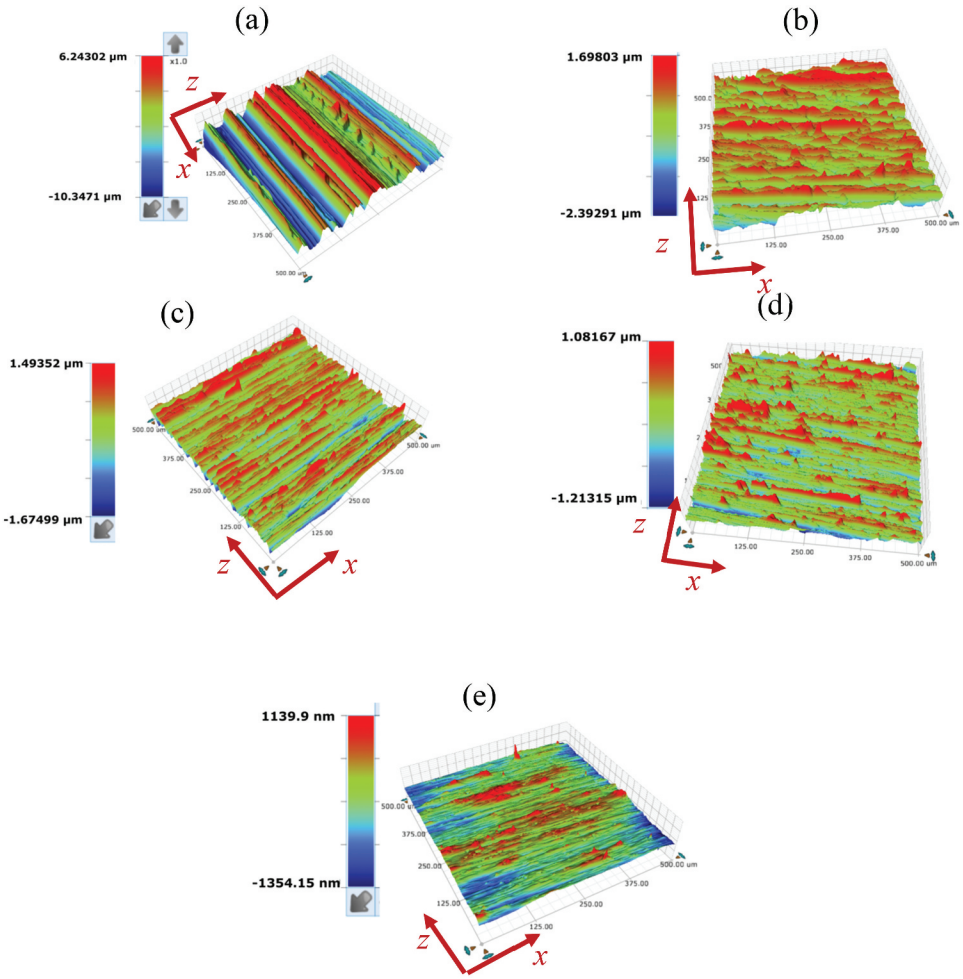

Figure 3. Typical 3D mapping (*500 µm* versus *500 µm*) for different abrasive paper: (a) P80, (b) P320, (c) P600, (d) P1200 and (e) P400 + diamond paste.

corresponding to a tracked adhesive failure initiation, can occur in two classical formats: corner failure initiation and central failure initiation (see Figure 6). The small round area is also surrounded by a tetrahedron-shape remaining adhesive.

In addition, Birro et al. (2021).[13] demonstrated that the overall behavior of the three-point bending specimens can be directly related to failure initiation area (S_c): stable propagation is expected for high S_c, whereas an unstable propagation is expected for low S_c. Besides, Birro et al. (2021).[13] demonstrated that cohesive failure might occur for outstanding surface treatments (STs).

A first step immediately after finishing a test is the visual post-mortem analysis, based on the classification described by Birro et al. (2021)[13]: adhesive initiation (central or at the corner), cohesive initiation, bulk failure, and complete adhesive failure. Indeed, the post-mortem identification is performed

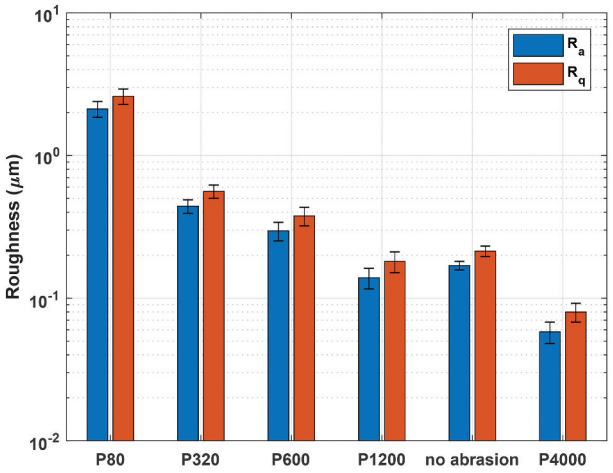

Figure 4. Roughness evaluation using different abrasive papers.

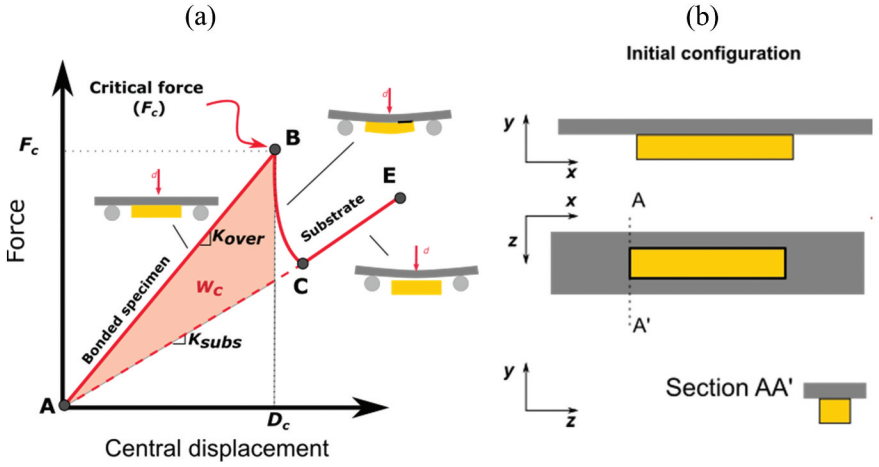

Figure 5. (a) Typical curve of 3PBT: AB –specimen stiffness; B –instantaneous failure initiation; BC – Failure Propagation; CE –substrate stiffness; (b) Reference planes before the failure initiation.

using the high-definition camera Nikon D3. The small round area is then analyzed to ensure an adhesive failure. In such a case, the assessment of failure initiation is performed via Scanning Electron Microscope (SEM) with Focused Ion Beam (FIB) (Dual SEM/FIB FEI HELIOS 600I) and 3D map scanning using a mechanical profilometer (DektakXT Stylus – Bruker Corporation).

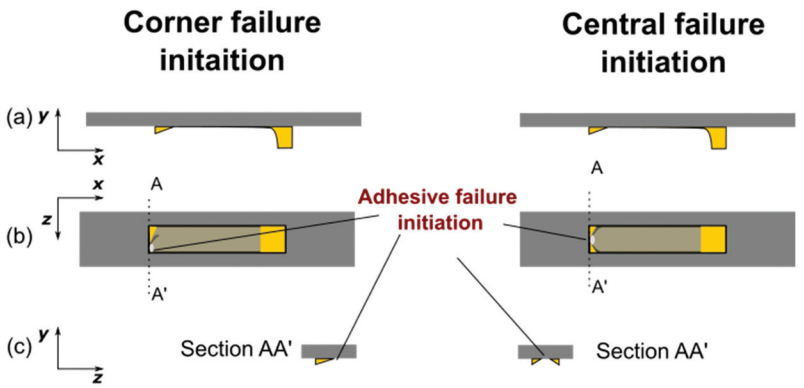

Figure 6. Typical positions of the failure initiation area: at the corner or central.

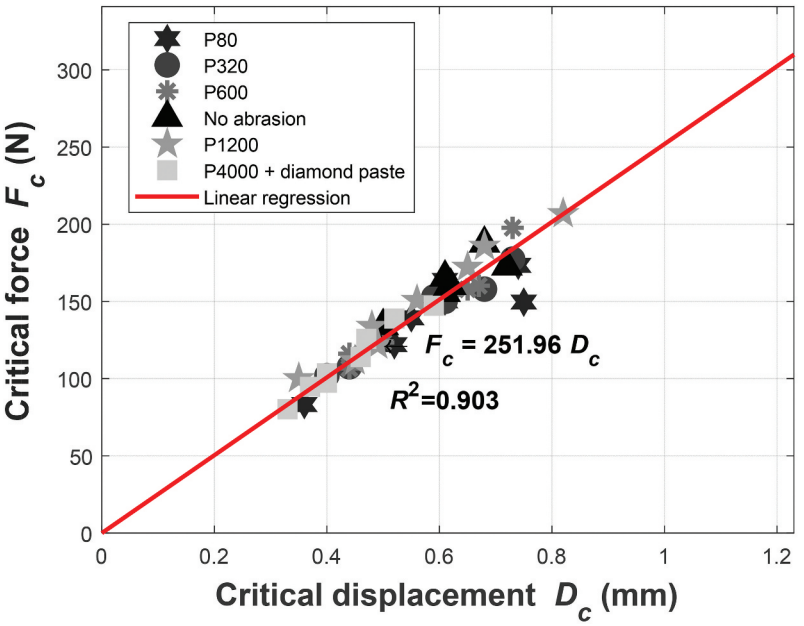

Figure 7. Critical force versus critical displacement for different roughness conditions.

2.4. Three-point bending test result

First, the critical force (F_c) and critical displacement (D_c) up to failure are recorded and plotted in Figure 7. A linear tendency between F_c and D_c appears when the mechanical ST varies, as expected. Sauvage et al. (2017)[15] had also found similar tendencies when different chemical STs were tested.

In special, each configuration's critical force (F_c) is plotted in terms of average roughness (R_a), as demonstrated in Figure 8. A similar tendency is reported, as also shown by different studies.[2,4,6] Nevertheless, the limited

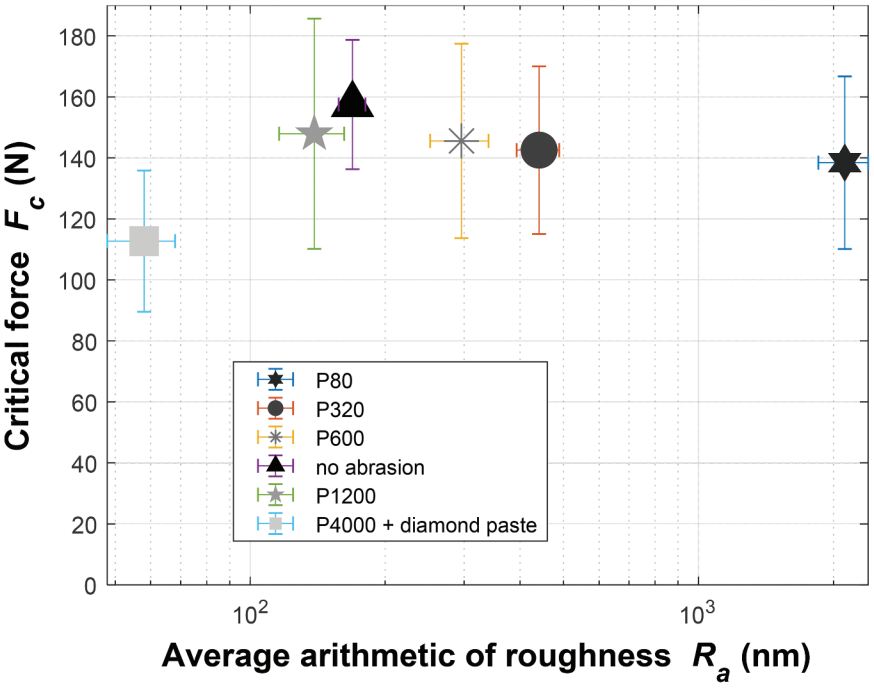

Figure 8. Critical force versus average arithmetic of roughness.

number of test cases and standard deviation intervals of experimental test results shown in the present study do not allow to determine the optimal roughness maximizing F_c.

For a complete evaluation, the failure initiation area of each sample is also measured using the methodology proposed by Birro et al. (2020)[13]: the number of pixels inside the failure initiation area of each sample is calculated using the software ImageJ. The corresponding failure area is computed using proportionality, comparing the number of pixels inside a reference area ($1\ mm^2$), as performed in the previous works.[13,14] In addition, only the central and corner initiation failures are obtained in the present works, as demonstrated in Figure 9. As performed by Sauvage et al. (2017),[15] a practical criterion is established for cataloging a central failure initiation area: the small round zone is allocated over two-thirds of the central width.

Although a classical adhesive failure initiation area (central or corner failure initiations) is present for the lowest roughness, the failure initiation cannot be distinguished from propagation, as demonstrated in Figure 10.

Finally, the relation between F_c and S_c is constructed (see Figure 11), as previously described by Birro et al. (2021).[13] Thus, the result obtained for the abraded substrate is in agreement with the typical curve obtained via pure chemical treatment.[13] In addition, even though the failure initiation area is not present for the group "P4000+ diamond paste," the curve's distribution is

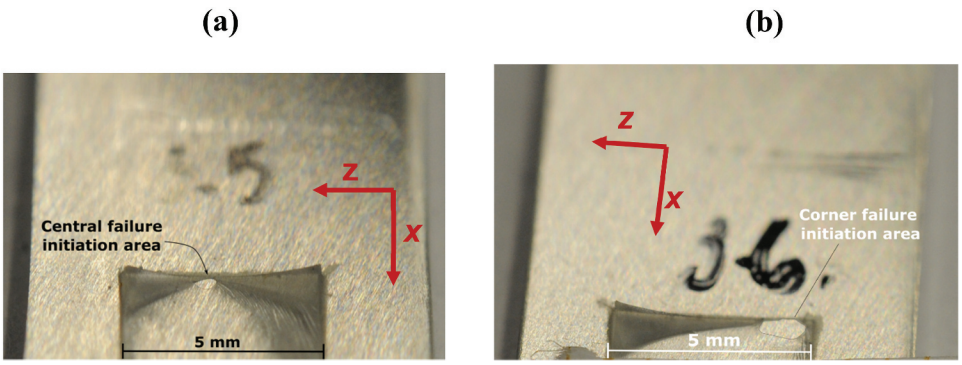

Figure 9. Typical failure initiation areas –(a) central failure initiation, (b) corner failure initiation.

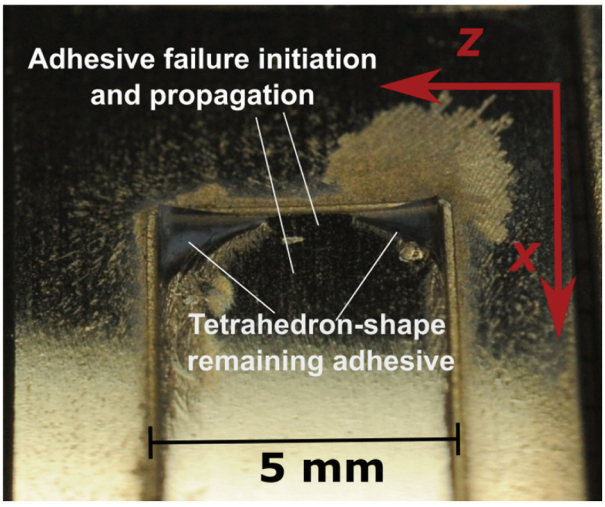

Figure 10. Adhesive failure initiation and propagation obtained for the configuration P4000 + diamond paste –No small round area is tracked, although a similar fracture shape is obtained (see Figure 9 -a).

estimated using the standard deviation obtained for F_c. In such a case, the solid blue line represents the average force (F_{P4000}) for the group "P4000+ diamond paste". The dashed and the dotted blue lines represent the average force (F_{P4000}) plus the standard deviation (SD) and the average force (F_{P4000}) minus the standard deviation.

3. Evaluation of adhesive failure initiation zone

By definition, a theoretical adhesive (interfacial) failure occurs when the first layer of bonds between the adhesive and the substrate is broken.[16] Nevertheless, Packham (2011)[1] argued that adhesive failure might be rare, but it can occur sometimes. On the other hand, a failure is considered cohesive if the adhesive is separated from the substrate on an adhesive layer sufficiently far from the

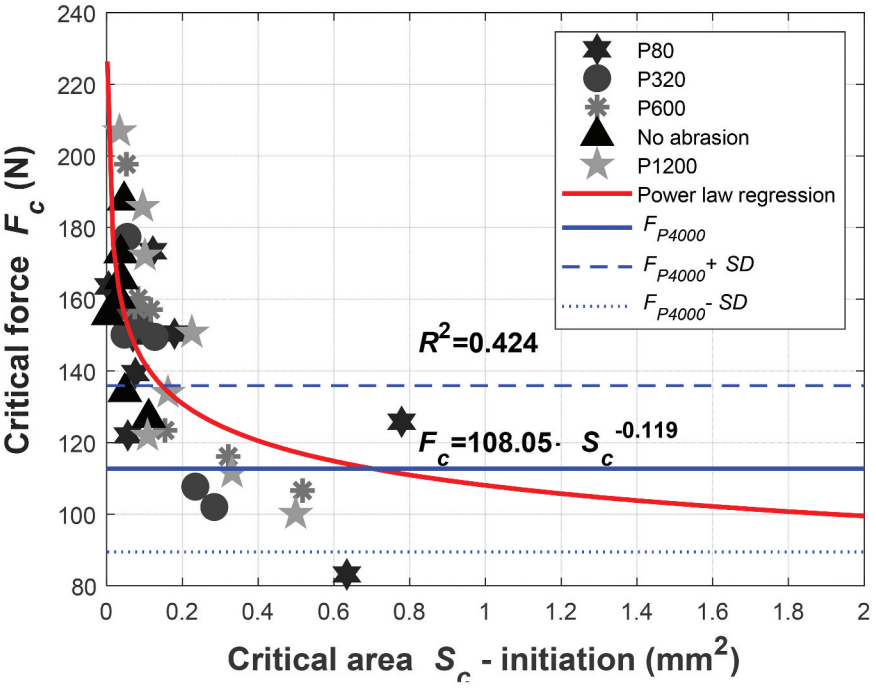

Figure 11. Critical force (F_c) versus failure initiation area (S_c) for different abrasion conditions.

interface, which means that the properties do not vary through the adhesive thickness. Else, an interphasial failure is assumed if the adhesive separates from the substrate on a layer whose properties differ from the bulk polymer. For the specific case of DGEBA/DETA and aluminum alloy, Aufray et al. (2005)[17] have demonstrated that interphase can reach a size up to 300 μm for a contact duration greater or equal to 3 hours at room temperature. Therefore, the specific condition set in Section 2.1 (contact duration, room temperature, and atmospheric pressure) ensures that similar and stable interphases are reached for all samples and the only parameter modified is the roughness profile.

In fact, the theoretical definition of adhesive failure is exquisite, and therefore, such a criterion is not practical since it requires robust measurement techniques. Besides, a model surface, which represents a surface with no roughness profile, is not a simple task to get, even less in the presence of an ST. Thus, a clear distinction of the residual adhesive layer from the substrate roughness is not simple. A practical criterion of adhesive failure is analyzed hereafter.

3.1 FIB

A first step immediately after finishing a test is the visual post-mortem analysis, based on the classification shown in Figure 8. For ensuring that a "small round area" corresponds to an adhesive failure, the failure initiation is assessed via Scanning Electron Microscope (SEM) with Focused Ion Beam (FIB).

Thus, for evaluating in locus the adhesive-to-cohesive failure transition, a specimen of the group P1200 is analyzed. In special, this group of samples possesses the lower roughness whereby failure initiation area can be identified. Since the samples are abraded by a controlled rotation of the abrasive paper, the orientation of rotation marks can vary over the substrate (see Figure 12). Nevertheless, the direction of rotation marks does not impact the roughness parameters since they are calculated over an area instead of a line. In this way, the failure initiation area (small round area) is then analyzed in locus, as shown in Figure 12.

The residual adhesive layer is then analyzed using a Dual SEM/FIB FEI HELIOS~600I at Microcharacterization Center Raimond Castaing. First of all, a carbon layer is deposited over the post-mortem surface. When the select area for cutting is defined, a local platinum deposition is performed for extra protection, followed by the ion cutting process. In such an analysis, a cross-section along and through a rotation mark (surface valley) is analyzed using Focused Ion Beam (FIB) milling (Ga^+ ions) (see Figure 13).

When the valley region is analyzed, two distinct zones are noticed (see Figure 14). An almost straight failure initiation is obtained on the lower side. In this zone, only the carbon layer deposition plus a lower residual adhesive layer is present.

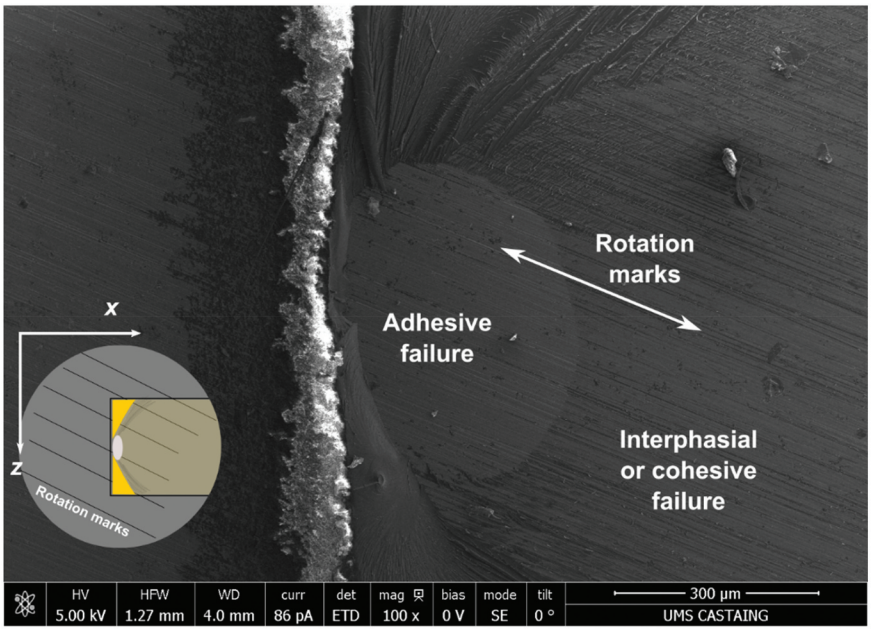

Figure 12. SEM of adhesive failure initiation –P1200.

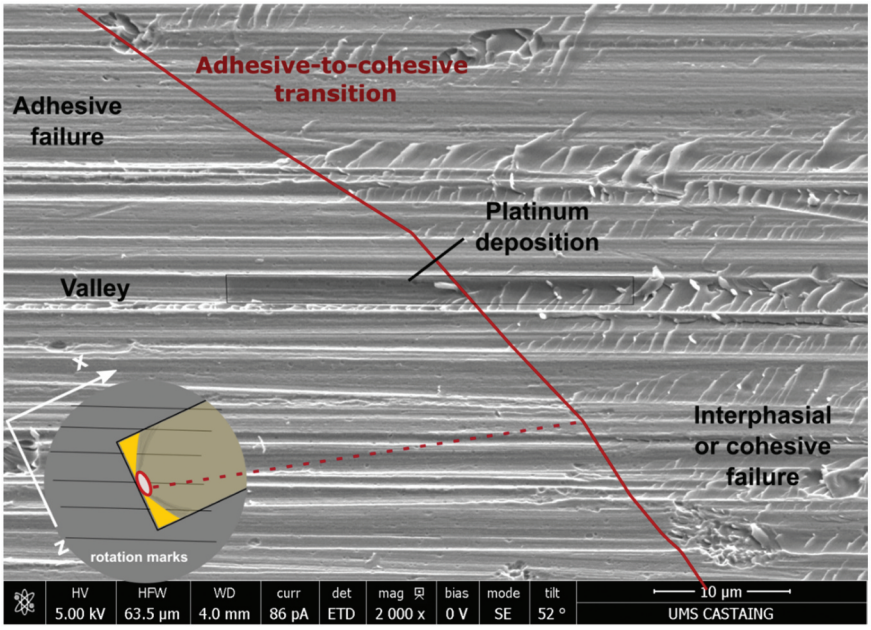

Figure 13. Cutting process along a rotation mark (valley) performed via Focused Ion Beam (FIB) milling (Ga+ ions). –P1200.

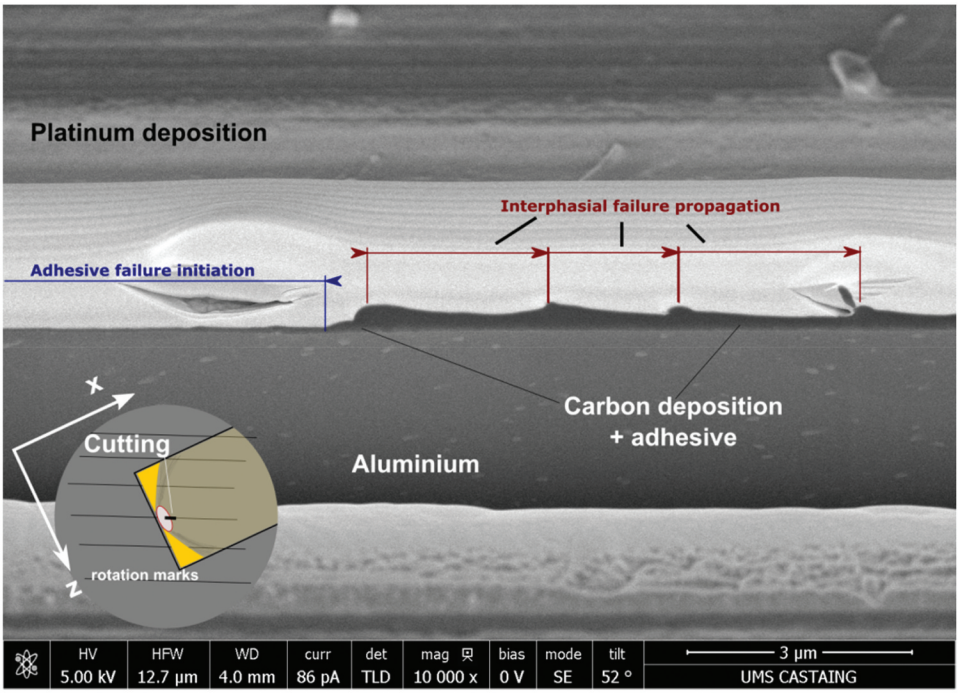

Figure 14. Adhesive-to-interphase transition failure along a valley.

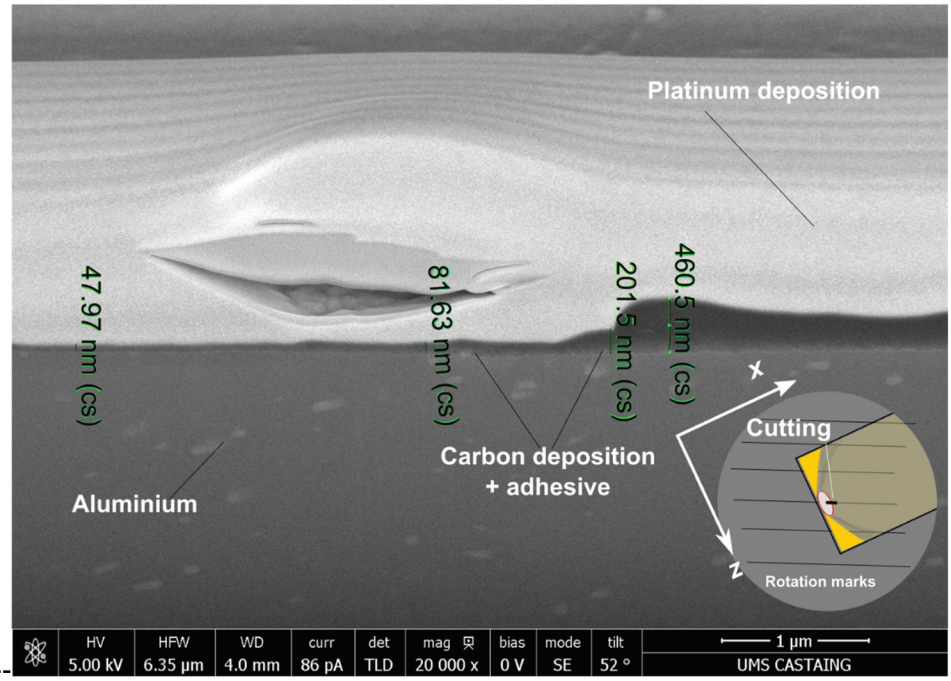

Figure 15. Height of carbon deposition and residual adhesive layer throughout a valley.

Therefore, the residual adhesive layer possesses a variable thickness throughout the "wave-shape" propagation (see Figure 15). Even if failure propagation may not manifest itself macroscopically (i.e., unstable propagation, as discussed by Birro et al. (2021)[13]), the crack step can be assessed at a microscopic level. Nevertheless, the corresponding load drop for the micro crack step is not possible to be measured yet.

In conclusion, the SEM+FIB analysis demonstrates that the visual post-mortem analysis can be considered an adhesive failure when a suitable criterion is adopted. As a significant advantage, the optical measurements described in Section 2.3 require much less preparation than a costly and complex FIB analysis.

In addition, a region far from the failure initiation area is also analyzed using SEM and FIB, as shown in Figure 16. As can be seen in SEM analysis (see Figure 17), the post-mortem analysis reveals that the adhesive is peeled off from adhesive asperities. The wave-shape propagation is also present, corresponding to a typical mode I fracture behavior.[18] The failure mechanism makes one think of a "peel test" in microscale, where the adhesive works as a flexible adherend and the substrate as a rigid adherend.

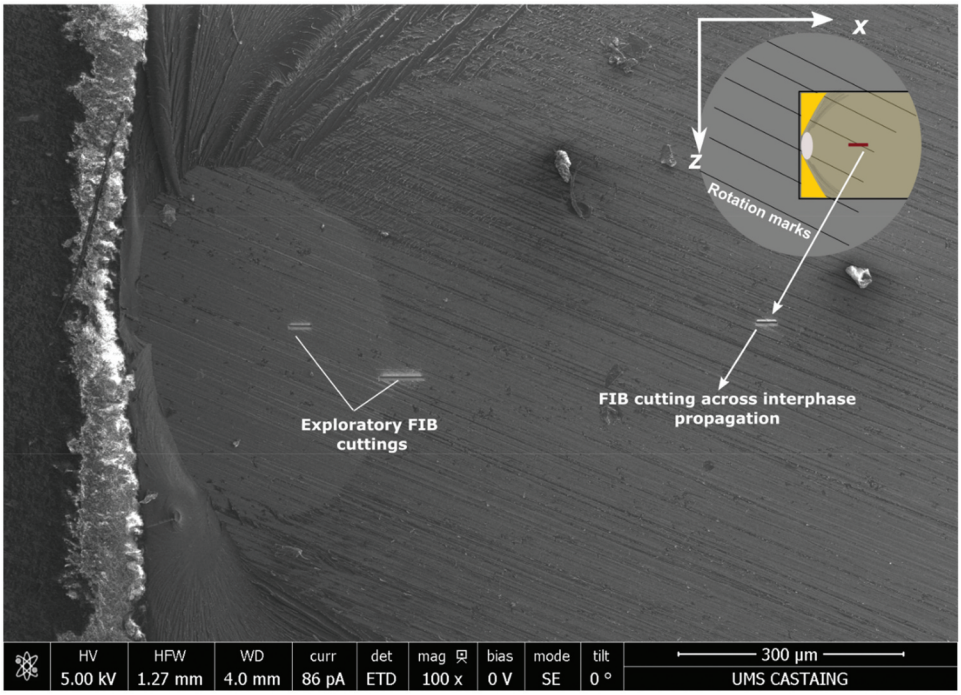

Figure 16. SEM of an interphasial failure propagation–FIB cutting is performed across interphase (on the right side).

In addition, the residual adhesive layer is analyzed throughout the roughness profile, which comprises peaks and valleys. As shown in Figure 17, a thicker carbon layer is interlocked at the valleys, and no significant carbon layer is found surrounding the roughness profile (see Figure 18).

As shown in Figure 19, the residual adhesive layer that corresponds to an interphase failure has a variable thickness. In fact, a thicker residual adhesive layer is located into roughness valleys, whereas a thin layer surrounds the other elements of the roughness profile. Therefore, the thickness of the residual adhesive layer into the roughness valley is measured, as shown in Figure 19. For the specific case shown in Figure 19, the interphasial failure could reach a size up to *456 nm*.

3.2. Profilometer

The transition region that delimited failure initiation from propagation is analyzed in detail. Hence, 3D mappings are carried out to assess initiation-to-propagation transition, using the mechanical Profilometer DektakXT Stylus (Bruker Corporation), as presented in Section 2.4. Thus, the 3D mapping of the failure initiation area represented in Figure 12 is shown in Figure 20.

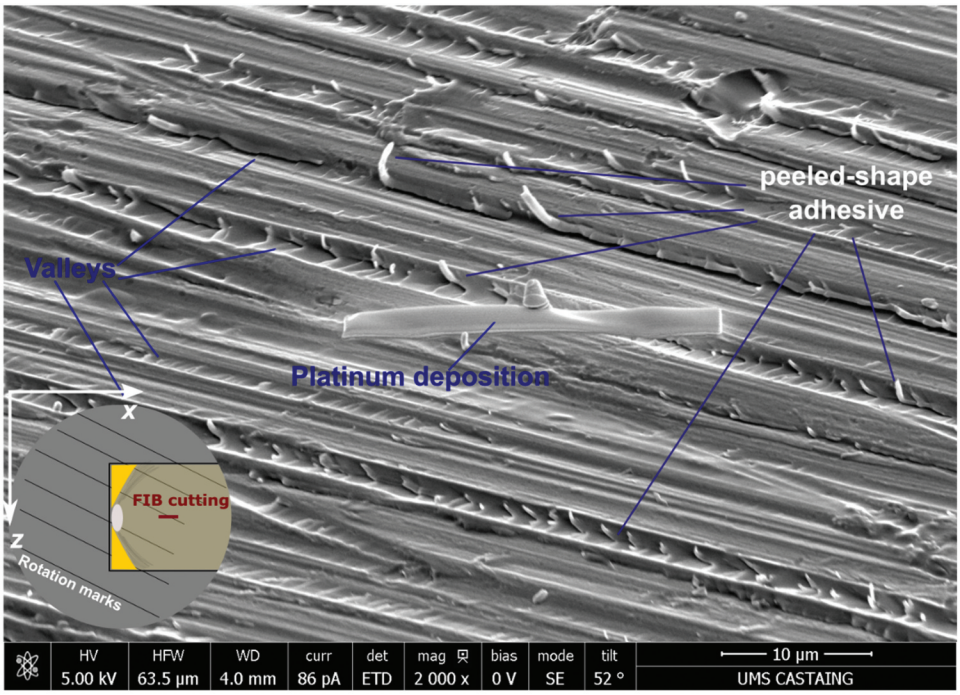

Figure 17. SEM of a post-mortem interphasial failure propagation and the analyzed region via FIB (P1200).

Nevertheless, a large scale is required to analyze the entire initiation-to-propagation transition thoroughly. For an accurate Profilometer analysis, a specific zone is considered for a more detailed analysis (50 µm x 80 µm) – pink rectangle in Figure 20.

As shown in Figure 21, the interlock mechanism can be better visualized when a local assessment of the initiation-to-propagation zone is performed. The residual adhesive layer is more concentrated into asperities, and a wave-shape propagation can be seen in Figure 22.

3.3. Practical criterion for defining adhesive failure

Thus, a general sketch of the adhesive bonding mechanism is shown in Figure 23. Birro et al. (2021)[13] suggested a practical criterion in terms of roughness to classify the three different failure mechanisms (adhesive, interphasial and cohesive failures). Thus, an adhesive failure was assumed if the residual adhesive thickness Δy_{res} is less than R_a. Therefore, the present works promote a forward step since the local assessment of the adhesive failure initiation zone demonstrates that the adhesive majority interlock into the valley region of rugosity, as shown in Figure 23. Thus, the residual adhesive

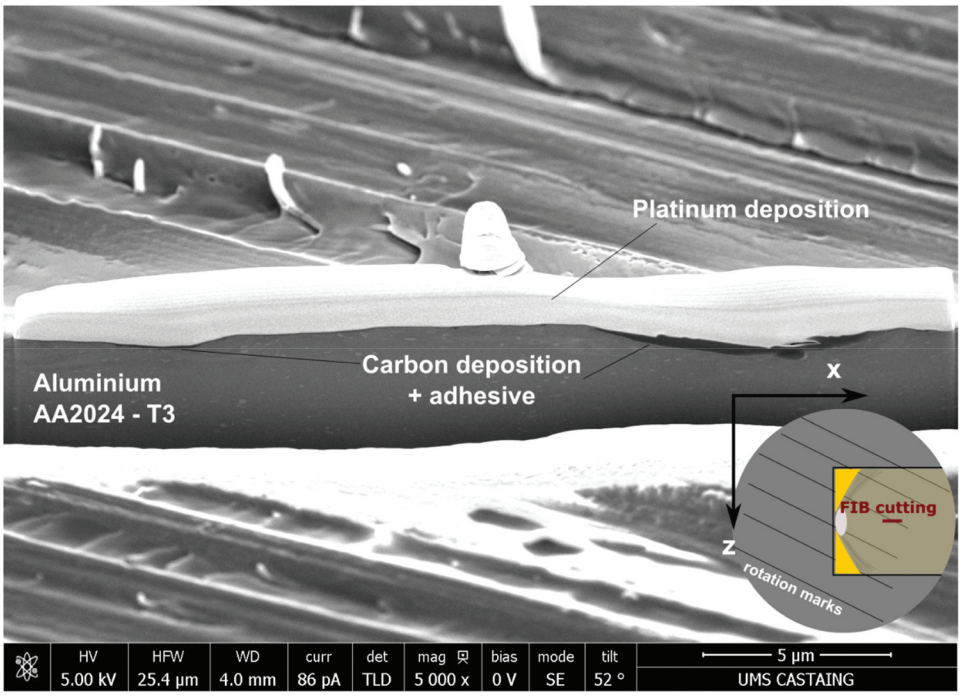

Figure 18. A FIB cutting across interphasial failure propagation–adhesive interlocked mostly at roughness valleys.

thickness has the order of magnitude of R_a. However, when R_a is very low (group P4000), the residual adhesive layer cannot interlock into asperity, and thus the failure initiation-to-propagation is no more identifiable. Even so, the failure initiation mechanisms have been shown as an interface debonding.

Therefore, based on the previous characterization of DGEBA/DETA and aluminum alloy performed by Aufray et al. (2005),[17] an interphasial failure is assumed if the residual adhesive thickness is comprised from the order of magnitude of R_a to *300 µm*. If the thickness of the residual adhesive thickness is greater than 300 µm, a cohesive failure is assumed. Other practical criteria of adhesive failure must be addressed for different combinations of adhesive and substrate since each adhesive-substrate combination has its own interphase thickness.

4. Statistical analysis of failure initiation mechanism – Weibull analysis

For a complete assignment of roughness influence, the critical force and the failure initiation area distribution are analyzed for each roughness condition. In special, the Weibull distribution is widely applied to describe brittle failures

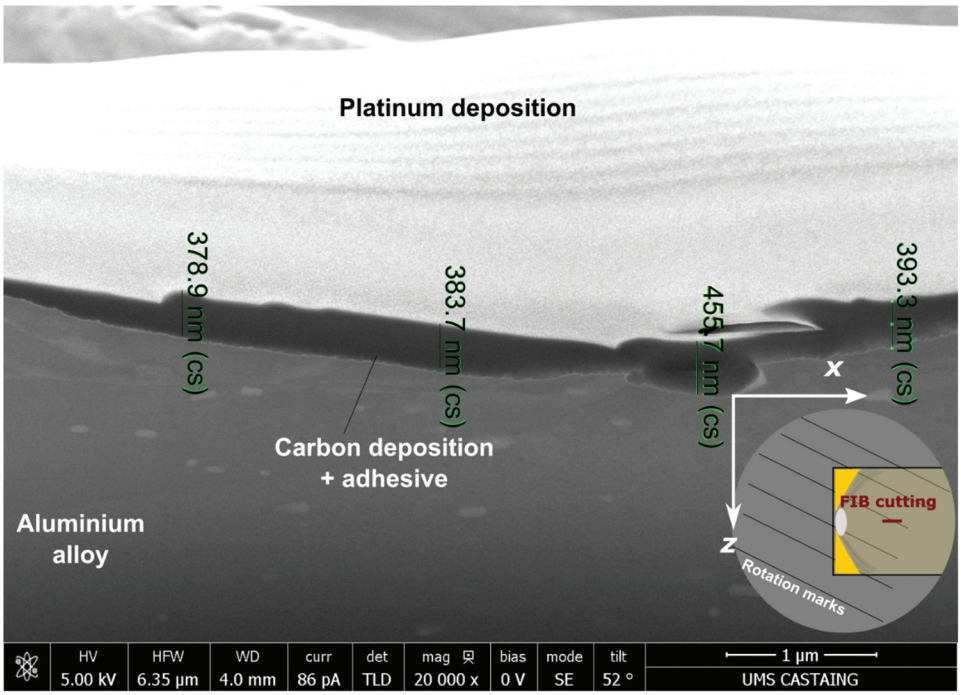

Figure 19. FIB cutting across interphasial failure propagation–a variation of the residual adhesive thickness into a roughness valley.

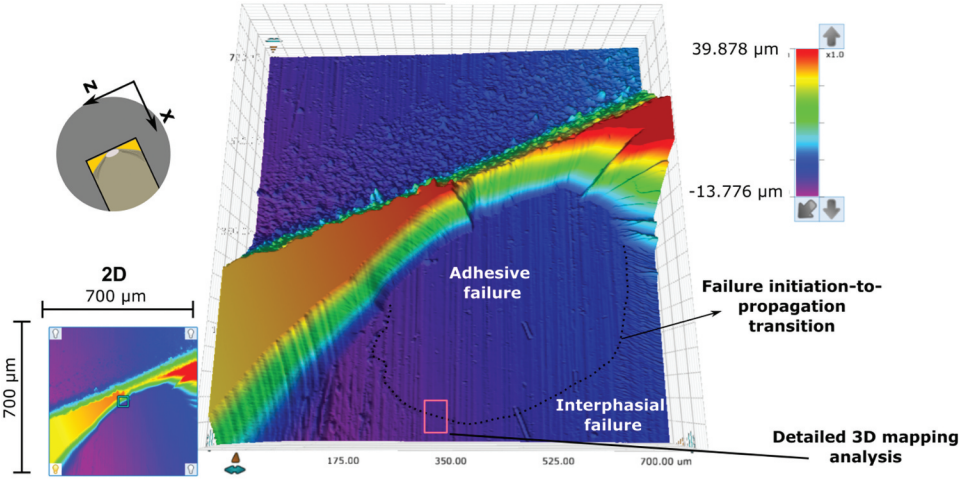

Figure 20. 3D mapping of a central small round area, as shown in .Figure 12

for many engineering problems.[19] The probability distribution function (PDF) and the cumulative distribution function (CDF) – also interpreted as the probability of failure – are expressed by Equations 1 and 2.

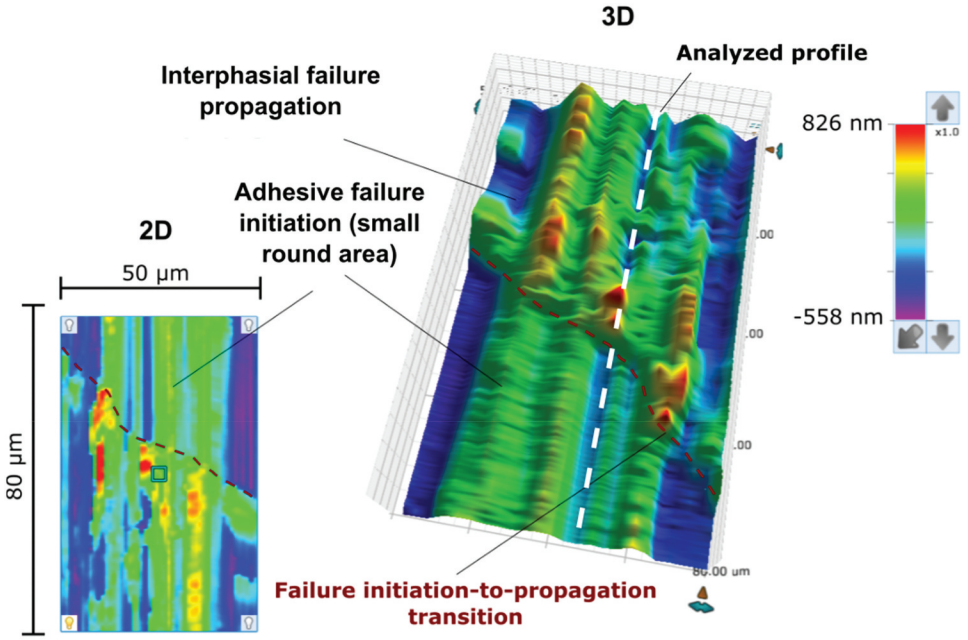

Figure 21. Zoom close to initiation-to-propagation zone–a pink rectangle of .Figure 20

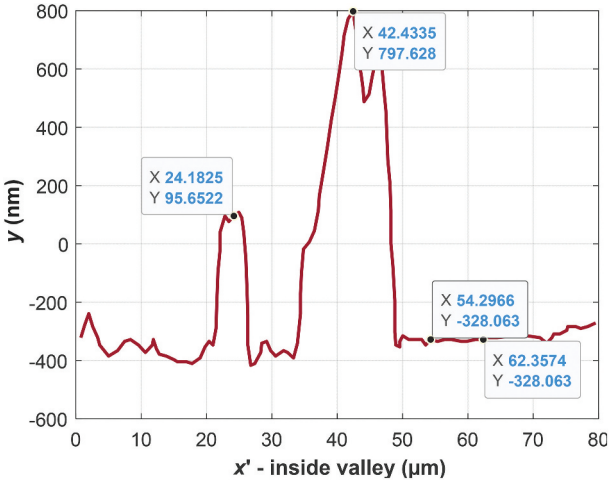

Figure 22. Wave-shape profile inside an asperity–white line of Figure 21 (valley region of roughness.

$$PDF \quad \frac{m}{\gamma}\left(\frac{F}{\gamma}\right)^{m\ 1}\exp\left(\ \ \left(\frac{F}{\gamma}\right)^{m}\right) \tag{1}$$

$$CDF \quad 1 \quad \exp\left(\ \ \left(\frac{F}{\gamma}\right)^{m}\right) \tag{2}$$

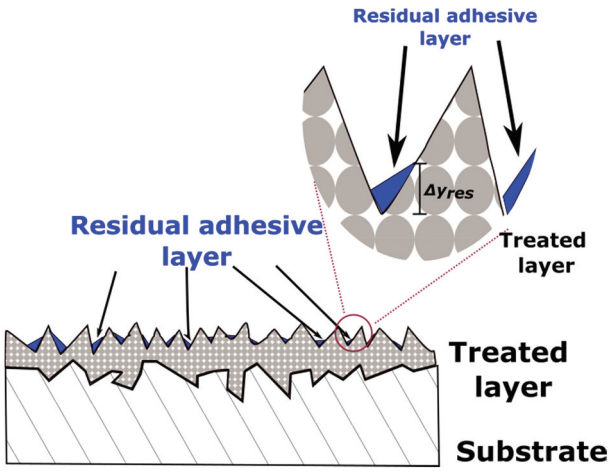

Figure 23. Residual adhesive layer interlocked into the asperities.

where m denotes the Weibull's modulus, and γ denotes a normalized factor (also known as the scaling factor). As discussed by Genty et al. (2017),[11] the Weibull's modulus indicates the variability in the strength of brittle materials, and thereby, the dispersion of defects decreases as the Weibull's modulus increases.

The estimation of Weibull parameters can be performed using different techniques, such as the least square method (LSM), the weighted least square (WLSM), the maximum likelihood method (MLM), and the method of moments. In special, Pobočíková and Sedliačková (2014)[20] demonstrated that WLSM and MLM last square method can outperform the others techniques for a sample size $5 < n < 15$. Considering the last mean square technique applied to fit both F_c versus D_c and F_c versus S_c, LSM is considered hereafter for Weibull's analysis. Thus, Equation 2 can be rewritten as a linear *log* equation as follows:

$$\ln(\quad \ln(1 \quad CDF) \quad m\ln(x) \quad m\ln(\lambda) \tag{3}$$

In the frame of LSM, different methods can be applied to estimate the probability of failure. In special, Bergman (1984)[21] indicated that the approach most reliable for a small group of samples is given as follows:

$$CDF \quad (j \quad 0.5)/n \tag{4}$$

where j denotes the label of the sample and n represents the total number of samples for each condition. Indeed, for Weibull's analysis, the variable must be ranked in ascending order.

When multiple failure modes are present, multiple Weibull's moduli are found when the CDF is plotted. Thus, using Equations 3 and 4, the term *ln(-ln (1-CDF)* in terms of *ln(Fc)* is plotted. In addition, the three types of failure

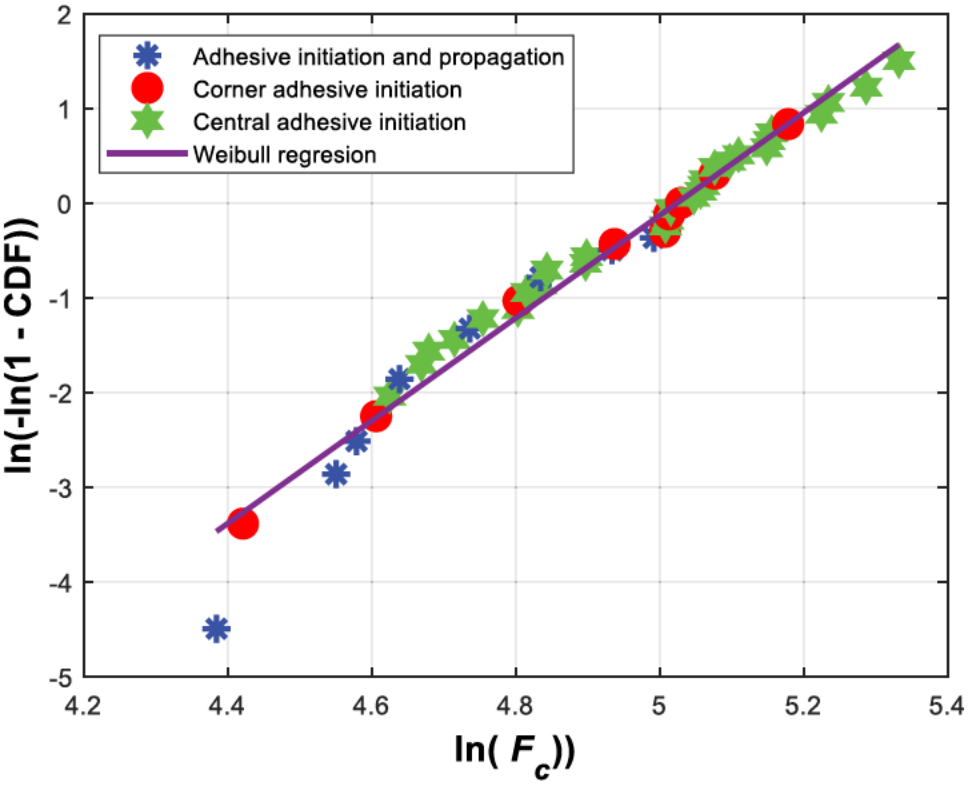

Figure 24. Weibull failure probability described by Equations 3 and 4 (*ln* versus *ln*) analyzing the mechanism of failure initiation.

initiation are identified by different colors, as shown in Figure 24. Thus, a good linear tendency is reported ($R^2 = 0.97$), which means statistically that all failure initiation modes are similar,[21] whatsoever the failure position (corner or central) or the failure propagation (interphasial or adhesive failure propagation).

Nevertheless, when the critical force becomes lower, the points seem more scattered when compared with the tendency line. This fact can be explained by the general failure initiation described by Birro et al. (2021). The small round area is no longer present for lower forces, nor the remaining tetrahedron-shaped adhesive. In such a case, Birro et al. (2021)[14] named as "complete adhesive failure", which means a pure adhesive failure along the entire overlap. Thus, the pure adhesive failure along the whole overlap can be considered a different failure mechanism, although the present work does not treat such a post-mortem analysis. The CDF is also plotted (see Figure 25), showing a good correlation.

Although a visual inspection cannot be used to track the initiation-to-propagation transition for a very low roughness, the statistical analysis performed via Weibull distribution ensures that the mechanism of failure

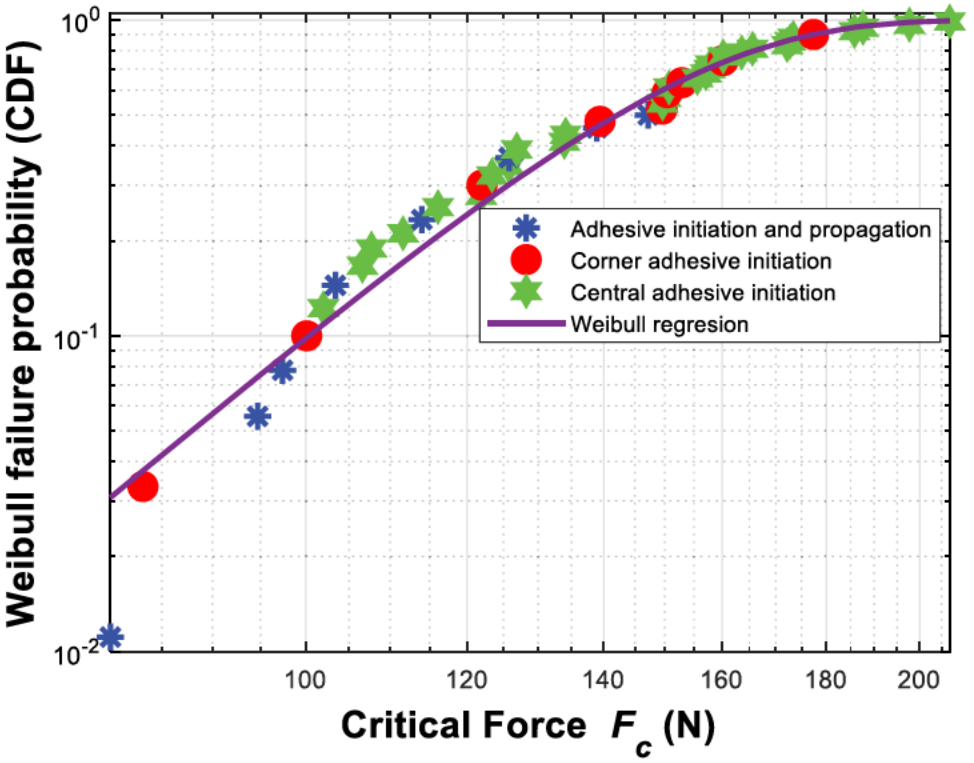

Figure 25. Weibull failure probability (Weibull distribution) and the fitted curve. A different failure initiation mechanism is manifested for low adherence (F_c).

initiation is the same. Nevertheless, a different failure mechanism is obtained during the crack propagation – interfacial failure propagation for a low roughness instead of an interphasial failure propagation for higher roughness. Therefore, a new fracture propagation mechanism is only reached when a low F_c is obtained experimentally, as previously constated by Birro et al. (2021).[14]

Thus, the experimental and statistical studies reveal that roughness can directly impact the critical length of failure initiation as well as the mechanism of fracture propagation when a low roughness is reached, even though all failure initiations are adhesive and independent in terms of roughness comprised from $58 \leq R_a \leq 2120$ *nm*.

5. Conclusion

In the present works, the effect of roughness (R_a) on the failure initiation is addressed in the frame of the three-point bending test. The present works constated an optimal roughness for adherence (critical force F_c), which possesses an interface debonding for all these cases. Although the post-mortem analysis demonstrates a visual interface debonding, the failure initiation area depends on R_a. A power-law regression can relate the critical force and the

Table 1. Surface roughness parameter for different abraded substrates.

Group	*P80*	*P320*	*P600*	*P1200*	*P4000 + diamond paste*	*Non abraded*
R_a *(nm)*	*2120* ± 270	*441* ± 48	*296* ± 44	139 ± 23	*58* ± 10	*172* ± 15
R_p *(nm)*	*7220* ± 1050	*2264* ± 543	*1644* ± 291	1219 ± 348	*1289* ± 479	*895* ± 253
R_q *(nm)*	*2600* ± 320	*561* ± 60	*377* ± 56	181 ± 30	*80* ± 12	*220* ± 19
R_t *(nm)*	*15370* ± 2280	*4683* ± 522	*3588* ± 559	2187 ± 212	*2651* ± 489	*3168* ± 319
R_v *(nm)*	*−8150* ± 1780	*−2419* ± 302	*−1945* ± 559	−969 ± 190	*−1362* ± 115	*−2483* ± 247
R_k *(nm)*	*6680* ± 1440	*1379* ± 168	*0.938* ± 139	431 ± 71	*180* ± 36	*565* ± 34
R_{pk} *(nm)*	*2060* ± 1080	*435* ± 157	*0.329* ± 26	221 ± 37	*112* ± 16	*235* ± 36
R_{vk} *(nm)*	*2530* ± 830	*680* ± 153	*0.461* ± 121	201 ± 40	*75* ± 9	*283* ± 9

failure initiation area (S_c). For a more precise and safer adhesively bonded design, the dependence between F_c and S_c, an interval analysis is overtaken, defining the maximum and minimum intervals for the power-law regression. Finally, the failure initiation areas are also evaluated using a profilometer and a Scanning Electron Microscope (SEM) with a Focused Ion Beam (FIB). Thus, an adhesive failure criterion based on the order of magnitude of R_a. In addition, a Weibull analysis reveals that both corner and central failure initiations have similar fracture mechanisms. Although the adhesive failure has been associated with an improper surface preparation of the substrate, the effect of increasing R_a is not sufficient to avoid an interface debonding, but it can indirectly affect the energy release rate during failure initiation. Thus, others texturing can be evaluated for better understanding and controlling adhesive failure initiation and propagation.

Acknowledgements

The authors gratefully acknowledge Occitanie Region and Université Fédérale de Toulouse Midi-Pyrénées ISAE-SUPAERO for the financial support These works were performed in the frame of the scientific network TACCOS, meaning Toulouse Adhésion Cohésion Collage Structural (https://personnel.isae-supaero.fr/eric-paroissien/taccos-557.html, http://maelenn.aufray.free.fr/taccos.php).

Disclosure statement

No potential conflict of interest was reported by the author(s).

Funding

This work was supported by the Région Occitanie Pyrénées-Méditerranée;ISAE-SUPAERO;

References

[1] Packham, D. E.;. 2011. Theories of Fundamental Adhesion. In *Handbook of Adhesion Technology*, Da Silva, L. F. M., Öchsner, A., and Adams, R. D., Eds., 587–609. Springer International Publishing: Berlin Heidelberg, doi:10.1007/978-3-319-42087-5_2-2.

[2] McBain, J. W.; Hopkinks, D. G. On Adhesives and Adhesive Action. *J. Phys. Chem.* 1925, *2*(2), 188–204. DOI: 10.1021/j150248a008.

[3] Ye, M.; Delplancke, L. J.; Berton, G.; Segers, L.; Winand, R. Characterization and Adhesion Strength Study of Zn Coatings Electrodeposited on Steel Substrates. *Surf. Coat. Tech.* 1998, *105*(1–2), 184–188. DOI: 10.1016/S0257-8972(98)00490-3.

[4] Packham, D. E. Chapter 7 - Surface Roughness and Adhesion. In *Adhesion Science and Engineering, Volume 2*, Dillard, D. A., Pocius, A. V., and Chaudhury, M. , Eds.; Elsevier Science B.V.: Amsterdam, 317–349, 2002; DOI: 10.1016/B978-044451140-9/50007-X.

[5] Cho, M. T.; Choo, Y. S.; Lee, M. J.; Oh, H. C.; Lee, B. C.; Park, T. H.; Shin, Y. S. Effect of Surface Roughness on the Adhesive Strength of the Heat-resistant Adhesive RTV88. *J. Adhes. Sci. Technol.* 2009, *23*(15), 1875–1882. DOI: 10.1163/016942409X12508517390671.

[6] Ghumatkar, A.; Budhe, S.; Sekhar, R.; Banea, M. D.; de Barros, S. Influence of Adherend Surface Roughness on the Adhesive Bond Strength. *Lat. Am. J. Solids Struct.* 2016, *13* (13), 2356–2370. DOI: 10.1590/1679-78253066.

[7] *ASTM D907-15 – Standard Terminology of Adhesives*; ASTM International: West Conshohocken, PA, 2015.https://www.astm.org/d0907-15.html

[8] Marinosci, V. M.; GRouve, W. J. B.; de Rooij, M. B.; Wijskamp, S.; Akkerman, R. Effect of Grit-blasting on the Fracture Toughness of Hybrid Titanium-thermoplastic Composite Joints. *Int. J. Adhes. Adhes.* 2021, *109*, 102893. in press DOI: 10.1016/j.ijadhadh.2021.102893.

[9] Paz, E.; Narbón, J. J.; Abenojar, J.; Cledera, M.; Real-Romero, J. C. Influence of Acrylic Adhesive Viscosity and Surface Roughness on the Properties of Adhesive Joint. *J. Adhes.* 2016, *92*, 877–891. DOI: 10.1080/00218464.2015.1051221.

[10] Roche, A.; Behme, A.; Solomon, J. A Three-point Flexure Test Configuration for Improved Sensitivity to Metal/adhesive Interfacial Phenomena. *Int. J. Adhes. Adhes.* 1982, *2*(4), 249–254. DOI: 10.1016/0143-7496(82)90032-X.

[11] Genty, S.; Sauvage, J. B.; Tingaut, P.; Aufray, M. Experimental and Statistical Study of Three Adherence Tests for an Epoxy-amine/aluminium Alloy System: Pull-Off, Single Lap Joint and Three-Point Bending Tests. *Int. J. Adhes. Adhes.* 2017, *79*, 50–58. DOI: 10.1016/j.ijadhadh.2017.09.004.

[12] ISO 14679. *Adhesives – Measurement of Adhesion Characteristics by a Three-point Bending Method*; International Organization for Standardization: Geneva, Switzerland, 1997.

[13] Birro, T. V.; Aufray, M.; Paroissien, E.; Lachaud, F. Assessment of Interface Failure Behaviour for Brittle Adhesive Using the Three-point Bending Test. *Int. J. Adhes. Adhes.* 2021, *110*, 102891. in Press. DOI: 10.1016/j.ijadhadh.2021.102891.

[14] Birro, T. V.; Paroissien, E.; Aufray, M.; Lachaud, F. A Methodology Based on the Coupled Criterion for the Assessment of Adhesive-to-adherend Interface Crack Initiation. *Int. J. Adhes. Adhes.* 2020, *102*, 102664. DOI: 10.1016/j.ijadhadh.2020.102664.

[15] Sauvage, J. B.; Aufray, M.; Jeandrau, J. P.; Chalandon, P.; Poquillon, D.; Nardin, M. Using the 3-point Bending Method to Study Failure Initiation in Epoxide-aluminium Joints. *Int. J. Adhes. Adhes.* 2017, *75*, 181–189. DOI: 10.1016/j.ijadhadh.2017.03.011.

[16] Kendall, K.;. 2002. Chapter 3 - Energy Analysis of Adhesion. In *Adhesion Science and Engineering*, Dillard, D. A., Pocius, A. V., and Chaudhury, M., Eds., 77–110. Elsevier Science B.V: Amsterdam, doi:10.1016/B978-0-444-51140-9.50030-5.
[17] Aufray, M.; Roche, A. A. Epoxy–amine/metal Interphases: Influences from Sharp Needle-like Crystal Formation. *Int. J. Adhes. Adhes.* 2007, *27*(5), 387–393. DOI: 10.1016/j.ijadhadh.2006.09.009.
[18] Arouche, M. M.; Budhe, S.; Banea, M. D.; Teixeira de Freitas, S.; de Barros, S. Interlaminar Adhesion Assessment of Carbon-epoxy Laminates under Salt Water Ageing Using Peel Tests. Proceedings of the Institution of Mechanical Engineers, Part L 2019. 233:1555–1563. 10.1177/1464420718766626.
[19] Bergman, B. On the Estimation of Weibull Moduls. *J. Mater. Sci. Lett.* 1984, *3*(8), 689–692. DOI: 10.1007/BF00719924.
[20] Pobočíková, I.; Sedliačková, Z. Comparison of Four Methods for Estimating the Weibull Distribution Parameters. *Appl. Math. Sci*. 2014, *8*, 4137–4149. DOI: 10.12988/ams.2014.45389.
[21] Beetz, J. C. P. The Analysis of Carbon Fibre Strength Distributions Exhibiting Multiple Modes of Failure. *J. Fiber. Sci*. 1982, *16*1, 45–59. DOI:10.1016/0015-0568(82)90015-X.
[22] ISO 4287:1997. *Geometrical Product Specifications (GPS) — Surface Texture: Profile Method — Terms, Definitions and Surface Texture Parameters*; International Organization for Standardization: Geneva, Switzerland, 1997.
[23] ISO 13565-2:1996. *Geometrical Product Specifications (GPS) — Surface Texture: Profile Method; Surfaces Having Stratified Functional Properties — Part 2: Height Characterization Using the Linear Material Ratio Curve*; International Organization for Standardization: Geneva, Switzerland, 1996.

Appendix A

For a global visualization of other roughness parameters,[22,23] the maximum peak height (R_p), the total height of the profile (R_t), the maximum valley depth (R_v), the core roughness depth (R_k), the Reduced peak height (R_{pk}) and the reduced valley depth (R_{vk}) are also listed in Table 1.